Starting the winter season: predicting endodormancy induction through multi-process modeling.

Guillaume Charrier

Starting the winter season: predicting endodormancy induction through multi-process modeling.

Guillaume Charrier[1]

[1]Université Clermont Auvergne, INRAE, PIAF, 63000 Clermont-Ferrand, France

*: corresponding author

Email: guillaume.charrier@inrae.fr

Tel: +33 4 43 76 14 21

UMR PIAF, INRAE Site de Crouel

5, chemin de Beaulieu

63000 Clermont-Ferrand

Abstract

In perennial plants, the annual phenological cycle is subdivided into successive stages whose completion will lead directly to the onset of the following one. A critical point is the transition between the apparent vegetative growth and the cryptic dormancy. To date, the initial date for chilling accumulation (D_{CA}) is arbitrarily set using various rules such as fixed or dynamic dates depending on environmental variables. These rules led to tremendous variability across studies and sites (from late summer until late autumn). To test the relevancy of different D_{CA}, we used a dataset combining dormancy release dates, budburst dates and frost hardiness measurements from 50 years in various orchards across France and Spain for *J. regia* cv Franquette. Many of the tested D_{CA} provided accurate results for the calibration and validation datasets (RMSEP < 10 and 8 days for endodormancy release and budburst dates, respectively). However, for frost hardiness, only the D_{CA} provided by the DORMPHOT model provided accurate results (RMSEP < 3°C). The best D_{CA} was thus selected using a composite index for all three processes. Testing the prediction under current and future climatic scenario showed that in, up to 25% of French territory under RCP 8.5 scenario, ecodormancy stage is likely to be delayed although temperature is decreasing. Overall, less average frost damages are expected although decennial risk (*i.e.* return period of ten years) is likely to increase in autumn in 15% of French territory. In southern part of France, delayed dormancy induction and release would induce delayed budburst and blooming altering flower and fruit production, whereas North East and Massif Central parts of France may suffer higher frost risks from late frost acclimation. Finally, this study describes relationships between climatic variables and plant phenological processes to build metamodels predicting next century's phenological cycles at the global scale.

Keywords: Chilling, Frost acclimation, Frost damages, Forcing, Photoperiod, Phenology, Risk assessment, Tree.

Introduction

In frost-exposed environments, deciduous trees have to timely adjust their biology and increase frost resistance by anticipating unfavorable conditions before the winter period. As observed for most stresses, avoidance and tolerance are two complementary processes driving frost resistance (Charrier *et al.*, 2011). The protection of shoot apical meristems under bud scales can be considered as an avoidance strategy. This is achieved through physiological changes allowing the transition from an apparently active (*e.g.* primary and secondary growth, leaf expansion, fruit maturation) towards a 'dormant' period (*e.g.* endodormancy and ecodormancy; Lang *et al.*, 1987). During this transition, different phenologically-related processes that are either visible (*e.g.* leaf fall, growth cessation, lignification or budset) or invisible (*e.g.* dormancy induction and release) take place. In parallel, trees transiently increase their frost tolerance through frost acclimation / deacclimation process (Charrier *et al.*, 2011).

In autumn, endodormancy release and frost acclimation are induced by the same environmental factors, namely decreasing temperature and photoperiod (Welling *et al.*, 2002; Arora *et al.*, 2003; Maurya & Bahlerao, 2017). After endodormancy was released, ecodormancy and frost deacclimation also occurs in parallel, under the control of warm temperature, in most species, eventually modulated by photoperiod in photosensitive species, such as late successional species (Basler & Körner, 2012). Process-based models using these variables as input have been developed to simulate the dormancy release and budburst dates (Chuine *et al.*, 2016), as well as frost hardiness (*e.g.* Leinonen 1996; Ferguson *et al.*, 2011; Charrier *et al.*, 2018).

Under the context of global change, it is particularly critical to accurately predict future trends in warmer climates. Since the first empirical model describing the relation between temperature and plant development, through the thermal-time concept (Réaumur, 1735), budburst and blooming models were only computing accumulation of growth-effective

temperature *i.e.* growth degree days (GDD). As the starting point was set at the coldest period of the year (*i.e.* January 1st or July 1st in northern and southern hemisphere, respectively), these models provided accurate results. However, this type of model was not efficient under warmer winter areas, where temperate crop species were attempted to grow (*e.g.* Northern Africa, Middle East or South America; Balandier *et al.*, 1993). In this context, temperate perennial crops did exhibit lack of chilling and insufficient endodormancy release (Weinberger, 1950). The process of endodormancy, and related chilling accumulation, had thus been introduced into models (Weinberger, 1956; Vegis 1964). In the recent decades, naturally growing trees have also been affected by a reduction in chilling exposure throughout winter, enhancing the interest into the endodormancy stage (Gauzere *et al.*, 2019).

Two-step models, simulating endo- and ecodormancy stages, are now commonly used to predict budburst dates (Chuine *et al.*, 2016). Frost acclimation models use similar formalism with direct linkage between frost acclimation and exposure to chilling temperatures followed by frost deacclimation and exposure to forcing temperatures, respectively. In perennial plants, the completion of a stage will directly drive the onset of the following ones (Hänninen & Tanino, 2011). However, the initial date for chilling accumulation (D_{CA}) is usually arbitrarily set with various rules leading to tremendous variability across studies (from late summer until late autumn). Four different concepts of D_{CA} have been used (see Tab. S1):

- Fixed date across years and locations: from September 1st (Chuine *et al.*, 2016) until November 1st (Weinberger, 1967), for northern hemisphere,
- Dynamic date through a simple climatic threshold: critical temperature (*e.g.* date of the first frost; Landsberg, 1974) or photoperiod (Welling *et al.*, 1997),
- Dynamic date through a mathematic function using a single variable such as the date of minimum chilling units computed by the Utah model (Richardson *et al.*, 1974),

- Dynamic date through a mathematic function using interacting variables (temperature and photoperiod) simulating leaf fall date (Delpierre *et al.*, 2009) or dormancy induction (DORMPHOT; Caffarra *et al.*, 2011a).

These different approaches have mainly been used for phenological cycle prediction. Thanks to a large dataset combining data from 50 years in various orchards across France and Spain for *J. regia* cv Franquette, we tested different formalism to compute the effects of the onset of chilling accumulation D_{CA} on the accuracy of three related processes (endodormancy, ecodormancy and frost acclimation/deacclimation). The optimal model was subsequently assessed for future climate prediction over France following three contrasted *scenarii*.

Material and methods

Endodormancy release and budburst dates

Endodormancy release dates were measured using the one-node-cutting 'forcing' test of Rageau (1982). Samplings were performed every three weeks from October until May and 48 one-node cuttings prepared per sampling date. Buds were isolated from other parts of plant to prevent correlative inhibitions (Dennis, 2003). At each sampling date, one-year-old stems were cut in 7-cm long pieces, bearing only one node at the top or less than 1 cm below the top end, for terminal and axillary buds, respectively. For axillary buds, the top of the cutting was covered by paraffin wax to prevent desiccation. The bases of the cuttings were immersed into tap water, weekly changed. Cuttings were exposed to optimal conditions for growth resumption (*i.e.* 16/8 D/N and 25°C) and individually observed every 3 days. Mean time until budburst (stage 09 BBCH) were computed from individual time until budburst for each cutting. After endodormancy release, buds of *J. regia* cv Franquette break out after 20 days under optimal conditions (Mauget, 1980; Charrier *et al.*, 2011). Endodormancy release dates were thus obtained by linear interpolation between the two dates giving a time to budburst higher (or equal

to) and lower (or equal to) than 20 days, respectively. Budburst in the field was monitored every two to three days in the different sites until 50% of buds reached the stage 09 of the BBCH scale.

Frost hardiness

Frost hardiness was measured from September until budburst on one-year-old branches in different orchards (Tab. 1) using the electrolyte leakage method (Charrier & Améglio 2011). Samples were cut into six 7-cm-long segments without buds and exposed to four different freezing temperatures among this set of temperatures: -5, -10, -15, -20, -30 and -40 °C. Depending on the season, either the highest or the lowest temperatures were not used. Two supplementary subsamples were exposed to control (+5 °C) and maximal freezing temperature (-80 °C). Freezing and thawing rates were set to 5 K h^{-1}.

Relative electrolytic leakage (REL) was calculated as (C1/C2) as described in Zhang & Willison (1987). We assumed a sigmoidal relationship between REL and temperature (θ) for each sample:

$$REL = \frac{a}{1+e^{b(c-\theta)}} + d \quad (1)$$

where parameters a and d define asymptotes of the function, and b is the slope at the inflection point c.

Frost hardiness was defined as the temperature of the inflection point (c) of the adjusted logistic sigmoid function (Repo & Lappi 1989), whereas frost sensitivity was considered to be estimated by the parameter b in percent damage per Celsius degree.

Climate data

Models were fit using observed daily mean and minimal temperature monitored by weather station, located most of the time in the same orchard and closer than 10km distance (Table 1).

For predictive purpose, the temperature, calculated according to the CNRM-ALADIN52 model and corrected by a Q-Q method (Déqué *et al.*, 2007), were used from 8462 sites across France (Safran grid at 8km spatial resolution; MétéoFrance). Four datasets were used as input variable: reference period (1950-2005) and three contrasted climatic *scenarii* (RCP 2.6, RCP 4.5 and RCP 8.5) for the future period (2005-2100). For each site and day, day and night length were computed depending on the latitude and day of year.

Endodormancy induction and onset of chilling accumulation

Date of the onset of chilling accumulation (D_{CA}) was computed through different functions:

i) Fixed D_{CA} every *ca.* 10 days from DOY 182 (July 1st) until DOY 335 (November 30th).

ii) Dynamic D_{CA} based on threshold values reached by minimum temperature (T_{min}), mean temperature (T_{mean}), first frost (FF) or photoperiod.

iii) Date of minimum chilling units (CU_{min}) were computed according to the Utah model (originally developed on *Prunus persica*) that computes negative chilling effect for temperature higher than 16°C (Richardson *et al.*, 1974). Daily CU started were summed from DOY 182 (July 1st) until DOY 365 (December 31st) using the Utah_Model function (ChillR package; Luedeling, 2019).

iv) Predicted leaf fall dates (BBCH 97) were computed according to the thermal (LFT) and photothermal (LFPT) models developed by Delpierre *et al.* (2009) and developed in *Quercus* and *Quercus* + *Fagus*, respectively. Below a critical photoperiod, temperature colder than a threshold, modulated by a photoperiod function in the case of the LFPT model, are summed up to a critical value (Y_{crit}), corresponding to the leaf fall date. Both LFT and LFPT model were computed using the original or a modified set of parameters: $LF(P)T_{ori}$ and $LF(P)T_{mod}$, respectively.

v) The dormancy induction state (DS) was computed according to the DORMPHOT model developed in *Betula pubescens* by Caffarra *et al.* (2011a). The two sigmoidal response

function to low temperature and photoperiod, respectively interact through sigmoidal functions. The original (DP_{ori}) and two modified (DP_E and DP_L, for early and late, respectively) sets of parameters were used.

Endodormancy release and budburst

Starting from D_{CA}, the sum of CU was modeled according to the inverse of the Richardson function (Richardson *et al.*, 1974) which was defined as the best function predicting endodormancy release dates in walnut trees (Chuine *et al.*, 2016; Charrier *et al.*, 2018). According to the sequential paradigm, the date where *CU*(*t*) reaches the critical threshold CU_{crit} (arbitrary chilling units, *CU*) is the date of endodormancy release (D_{ER}), or the transition between endodormancy and ecodormancy!

$$CU(t+1) = CU(t) + Max\big(Min\big(T_{high} - \theta(t); T_{high} - T_{low}\big); 0\big) \quad (2)$$

with *CU*(*t*), the chilling unit at day *t*, T_{high}, both the temperature above which CU equals 0 and the amount of CU when temperature equals T_{low} or lower; CU being linear between T_{low} and T_{high}.

The ontogenetic development during ecodormancy stage was modeled according to a sigmoid function (Caffarra *et al.*, 2011a). The date when *FU(t)* reaches the critical threshold FU_{crit} (arbitrary forcing units, *FU*) is the budburst date (D_{BB}).

$$FU(t+1) = FU(t) + \frac{1}{1+e^{-slp(\theta(t)-T_{50})}} \quad (3)$$

with *FU*(*t*), the forcing unit at day t, slp, the slope of the function at the temperature inducing half of the maximal apparent growth rate T_{50}.

Frost hardiness and frost damages

Frost hardiness and subsequent frost damages were computed using a photothermal model developed on *Pinus sylvestris* (Leinonen, 1996) and adapted on *Juglans regia* (Charrier *et al.*,

2018). Shortly, hardening ability (C_R) changes in relation to the different stage of the annual cycle (endodormancy induction, endodormancy release, ecodormancy and growth). During endodormancy and growth stages, C_R was set to 1 and 0, respectively. During endodormancy induction, C_R was either considered gradually increasing from 0 to 1 during the 30 days before the onset of chilling accumulation (Fixed D_{CA}). For simple dynamic D_{CA}, C_R was set to 0 until the threshold was reached (CU_{min}, FF, T_{min}, T_{mean} or Photoperiod). For models describing continuous process, C_R was defined as the ratio between the related variable and its critical threshold (LF, LFPT and DP models). From the interaction between hardening, temperature and photoperiod, a dynamic potential state of hardiness is computed throughout the year. Daily changes in actual frost hardiness (FH) tend to reduce the difference between potential state of hardiness and FH with a temporal lag (see complete description of the model in the original publication). Frost damages are computed on a daily basis through the relation between FH, frost sensitivity (FS, slope at FH) and minimum temperature θ_{min} as:

$$FD = \frac{1}{1+e^{FS(FH-\theta_{min})}} \quad (4)$$

Model calibration depending on the onset of chilling accumulation

Three different sub-models, namely endodormancy release, ecodormancy release and frost hardiness, were calibrated one after the other, as they were interrelated. To minimize sums of square between observed and predicted values, we used the nls function (Gauss-Newton algorithm), with different sets of starting values at minimum, average and maximum ranges of parameter realistic values.

For endodormancy release model, one parameter was optimized: CU_{crit} corresponding to the sum of chilling units to release endodormancy. The other parameters were set to the values defined by Chuine *et al.* (2016). The dataset was split into calibration and validation datasets

containing 18 observations from 6 sites and 16 observations from 5 sites, respectively (Table 1).

For ecodormancy model, one parameter was optimized: FU_{crit} corresponding to the sum of forcing units to break buds. The endodormancy model used to predict D_{ER} was the best from the previous step and the other parameters set to the values described in Charrier *et al.* (2018). The dataset was split into calibration and validation datasets containing 41 observations from 7 sites and 36 observations from 4 sites, respectively (Table 1).

For frost hardiness model, seven parameters were optimized: T_1, T_2, NL_1, NL_2, δ, τ and FU_{critR}. The endodormancy and ecodormancy models used to predict D_{ER} and D_{BB}, were the best from the previous steps and the other parameters set to the values described in Charrier *et al.* (2018). The dataset was split into calibration and validation datasets containing 60 observations (6 winter periods) from 2 sites and 51 observations (5 winter periods) from 5 sites, respectively (Table 1).

The quality of the fit and the predictive ability of the models depending on D_{CA} were assessed for calibration and validation datasets computing Root Mean Square Error (RMSE) and Predictive Root Mean Square Error (RMSEP), respectively:

$$RMSE(P) = \sqrt{\frac{\sum_{i=1}^{n}(\hat{y}_i - y_i)^2}{n}} \quad (5)$$

with $\hat{y}_i$ the predicted values for an observation *I* and y_i the observed values for an observation *i*

As the different D_{CA} provided contrasted results among models, we used a composite performance index defined as :

$$PI = \frac{RMSE_{endoD_i}}{max(RMSE_{endoD})} + \frac{RMSE_{ecoD_i}}{max(RMSE_{ecoD})} + \frac{RMSE_{FH_i}}{max(RMSEP_{FH})} + \frac{RMSEP_{endoD_i}}{max(RMSEP_{endoD})} + \frac{RMSEP_{ecoD_i}}{max(RMSEP_{ecoD})} + \frac{RMSEP_{FH_i}}{max(RMSEP_{FH})} \quad (6)$$

Results

Effects of D_{CA} on model accuracy

Fixed D_{CA} only had a relatively small effect on the quality of the fit ($12.3 < RMSE_{endoD} <$ 15.1 days; coefficient of variation CV = 6.8% for a 153 days range) and the predictive ability of D_{ER} ($8.3 < RMSEP_{endoD} < 11.8$ days; CV = 11.7%). Fixed D_{CA} between DOY 223 (Aug. 11th) and 274 (Oct. 1st) are relatively efficient to simulate CU accumulation with respect to D_{ER}. The effect of various D_{CA} on the prediction of D_{BB} was also relatively low for the quality of the fit ($7.1 < RMSE_{ecoD} < 8.6$ day; CV = 6.1%) and the predictive ability ($6.9 < RMSEP_{ecoD} < 8.1$ days; CV = 4.7%). A wider range of fixed D_{CA}, *i.e.* between 223 and 325 (Nov. 21st), similarly performed for D_{BB} prediction. Annual phenological cycle (D_{ER} and D_{BB}) was thus best predicted when D_{CA} was set to DOY 254 (*i.e.* Sep. 11th). For frost hardiness, fixed D_{CA} earlier than DOY 305 (Nov. 1st) provided highly efficient fit (RMSE < 2.0°C). However, the prediction was not accurate enough, as RMSEP was almost twice higher (3.2 < RMSEP < 3.9°C).

The D_{CA} returned by the various dynamic functions were highly different across France: from DOY 182 ± 5 to 312 ± 14 (median ± SD; Fig. 1A). Four groups of earliness can be defined: very early (T_{min} and photoperiod), early (DP_E, $LFPT_{mod}$, and LFT_{mod}), intermediate (CU_{min}) and late (LFT_{ori}, $LFPT_{ori}$, DP_{ori}, DP_L and FF). All the dynamic D_{CA} computed via different functions exhibited highly significant correlation with mean annual temperature of the site (Fig. 1B-D).

Simple temperature thresholds, such as T_{min} or T_{mean} did not provide accurate phenological (RMSEP > 11.5 and 8.0 days for D_{ER} and D_{BB}, respectively) nor FH prediction (RMSEP > 3.3°C; Tab. 1). The D_{CA} calculated via a photoperiodic threshold was relatively efficient to predict D_{BB} (RMSEP = 6.8 days), but not D_{ER} (RMSEP = 10.2 days) nor FH (RMSEP = 3.5°C).

The D_{CA} computed using the Utah function did not provide accurate prediction for any variable of interest (RMSEP = 14.1 days, 7.8 days and 3.5°C for D_{ER}, D_{BB} and FH,

239 respectively). The leaf fall thermal function (LFT), using either the original (LFT_{ori}) or the
240 modified sets of parameters (LFT_{mod}), was relatively efficient to predict D_{BB} (RMSEP = 7.23
241 days) but less efficient for D_{ER} and FH (RMSEP ≥ 9.2 and 3.2 for D_{ER} and FH, respectively).
242 The leaf fall photothermal function (LFPT) provided accurate predictions for phenological
243 dates (RMSEP ≤ 8.8 and 6.9 days for D_{ER} and D_{BB} respectively) but not for FH (RMSEP > 3.2
244 °C). The D_{CA} computed using the DORMPHOT function were the most efficient to predict D_{ER},
245 D_{BB} and FH, in the original and 'Late' versions of the function (DP_{ori}, and DP_L, respectively).
246 Finally, the performance index (PI) accounting for all the models and methods of computing
247 D_{CA} could not distinguish between DP_{ori} and DP_L (PI = 6.31).

248 Finally, the different processes exhibited contrasted thickness linkage with D_{CA}. For
249 ecodormancy, a wide range of fixed date (100 days range: Aug. 11th until Nov. 21st) and all the
250 computations using photoperiod as an input variable, provided good fit and predictive
251 accuracies ($RMSE_{EcoD}$ and $RMSE_{EndoD}$ lower than 8 and 7.6 days, respectively). Endodormancy
252 release was slightly more restrictive with the best predictions either provided by fixed calendar
253 dates (Aug. 11th until Oct. 1st) or dynamic functions integrating the interaction between
254 temperature and photoperiod (LFPT and DP). Frost hardiness was the most restrictive, with
255 excellent predictive accuracy when using D_{CA} computed by DORMPHOT model (DP_{ori} and
256 DP_L; RMSEP < 3.0°C) compared to all the other computations.

257 Although both DP_{ori} and DP_L performed almost equally for the three variables of interest
258 (D_{ER}, D_{BB} and FH), DP_L exhibited a slightly better correlation to predict the dynamic of Mean
259 Time until budburst (MTB) during the period of dormancy induction (R^2 = 0.262 and 0.282 for
260 DP_{ori} and DP_L, respectively; Figure 2). Furthermore, as FH was slightly better predicted using
261 DP_L (RMSEP = 2.6°C), D_{CA} predicted by this function was selected to predict the current and
262 future frost risks (Fig. 3).

263 *Predictions under current and future climates*

Using D_{CA} computed from DP_L endodormancy release dates under current climate exhibited a structured geographical pattern across France. Endodormancy release dates spanned over a 60 days range (Fig. 3A): earlier in mountain area (Early December) and later on the Mediterranean (Mid-February) and southwestern coasts (Late January). Budburst dates exhibited an opposite pattern over a 77 days range (Fig. 3B): from Mid-April in Southern and Western parts until late June in mountainous area. Endodormancy release and budburst dates were highly correlated to mean annual temperature, although through different functions (exponential and cubic function for endodormancy release and budburst, respectively; Fig. 3C-D).

The geographic structure was less obvious for frost damages, with very low predicted damages during autumn (Fig. 4A) and spring (Fig. 4C), except in high mountain area. During the winter period, higher frost damages are predicted in the northeastern part of France (Burgundy, Alsace, Lorraine), in mountain areas and in the north of Rhone valley (Fig. 4B). Average predicted damages in autumn and spring were highly correlated to the date of first (<-4°C) and last frost event (< 0°C), respectively (Fig. 4D; F), whereas maximum winter damages were correlated to absolute annual temperature (Fig. 4E).

Similar trends are observed under future climate predictions, with high delay in both the onset of dormancy and release for mean annual temperature higher than 5°C (Fig. 5A, B). However, the delay affecting endodormancy stage does not carry over toward budburst with earlier budburst with increasing temperature for lower mean annual temperature than 10°C (Fig. 5C). It should be noted that similar or earlier budburst is likely to happen for higher temperature, and this may be observed in up to one quarter of France at the end of the XXIst century: from 5 (RCP 4.5) to 27% (RCP8.5 scenario) of the French territory in 2051-2100 (Fig. 6). Although such a delay is not forecasted within the 'Noix de Grenoble' Protected Designation of Origin area, budburst would be delayed in most of the 'Noix du Périgord' area under RCP8.5 scenario

(75.1% 2006-2050 and 94.2% 2051-2100). Overall, frost damages are expected to decrease, on average, all over France (Fig. S1). However, in North East and Massif Central, higher decennial risks are predicted under RCP 2.6 *scenario* (2006-2051; Fig. S2).

Discussion

Defining the initial date for cyclical processes is a critical issue. To predict annual phenological cycle in perennial organisms, such as trees, various empirical rules have been used so far. The onset of chilling accumulation during endodormancy stage (D_{CA}) had, for instance, been arbitrarily set using fixed dates across years and locations (Chuine *et al.*, 2016) or, under the dependence of environmental factors controlling the induction of dormancy (Caffarra *et al.*, 2011b). In the current study, we used long-term observations of phenological stages (endodormancy release and budburst) and related processes (frost acclimation and deacclimation) in various environmental conditions and showed that the DORMPHOT model was the most relevant to predict winter biology in walnut trees.

Depending on the studied process, not all computation performed equally (Tab. 2). The effect of D_{CA} on ecodormancy and budburst was buffered during endodormancy release. From a budburst perspective, various rules for D_{CA} computation can thus be considered as valid, although they all consider a potential effect of photoperiod, either directly or indirectly via fixed date (Welling *et al.*, 1997; Chuine and Régnière, 2017). A narrower range of fixed date and fewer dynamic computations of D_{CA} (DORMPHOT and LFPT models) provided accurate predictions for endodormancy release dates. However, providing predictive rules only based on one or two phenological stages, even though with a large number of measurements (more than 100 dates, combining endodormancy and budburst, in the present study) does not provide sufficient details for continuous process modeling. Introducing frost hardiness as a co-variable of dormancy induction and release provided higher temporal resolution into these concurring

processes (Welling & Palva, 2006; Charrier *et al.*, 2011; Hanninen, 2016). Through a multi criterion analysis, the D_{CA} simulated by the DORMPHOT model provided the most accurate predictions. This model, originally developed in *Betula pubescens*, is thus relevant for other deciduous species such as *Juglans regia*. The conceptual development of this model is indeed based on experimental results combining photoperiod and temperature manipulation (Caffarra *et al.*, 2011b), whereas other formalisms were based on empirical observations (*e.g.* leaf fall). Photoperiod and temperature are intimately related in controlling annual weather dynamics. However, temperature fluctuation is much higher at a given date of the year which could induce high variability in the onset of the winter season (see *e.g.* Fig.1). Since dormancy induction and frost acclimation are lengthy processes (*e.g.* ca. 1-2 month), perennial plants cannot only rely on temperature changes that can be too sudden for the onset of winter rest (Caffarra *et al.*, 2011a). Both photoperiod and temperature variables thus affect annual phenological cycle in perennial plants, although at different ratio across species. Photoperiod is for instance predominant in *Populus sp* (Kalcsits *et al.*, 2009) and *Vitis sp* (Fennel & Hoover 1991), while temperature in *Malus sp* and *Pyrus sp* (Heide & Prestrud, 2005) and *Sorbus sp* (Heide, 2011). The interaction of both photoperiod and temperature has been showed in *Prunus sp* (Heide 2008). Integrating both variables is an interesting strategy to prevent dormancy induction during cold late summer (without frost risks) while maintaining physiological activity under extended warm periods. It has been hypothesized that the modulation of photoperiod sensitivity by temperature may be related by thermal effect on phytochrome perception of day length (Mølmann *et al.*, 2005).

The selected rule for D_{CA}, predicting a delayed chilling accumulation in warmer locations (> 7°C MAT; Fig. 1C; 5A) would further delay endodormancy release in such area (Fig. 3 A, C). However, cold weather would limit ontogenetic development during ecodormancy, providing a negative picture of D_{ER} vs D_{BB} (Fig. 3). Under future climatic conditions such as

predicted by RCPs *scenarii*, this picture is likely to be blurred as the tipping point for budburst would be achieved (*ca.* 14°C MAT). Below 14°C, endodormancy would be released and warmer temperature of the winter-spring period lead to earlier budburst.

Date of first frost (< 0°C), minimum temperature and date of late frost (<-4°C) appear as good proxies to predict early, maximum and late frost damages, respectively (Fig. 4D-F). Predicted minimal temperature are expected to decrease as well and, even though flushing buds would be highly vulnerable to late frost, they are likely not to be exposed to damaging temperature (Fig. 4). Although climate models agree on the average trend, they are still unclear on the climate extreme events such as early and late frost events. Notably, the decennial damages (*i.e.* maximum damage occurring every ten years) may increase in North East and Massif Central area (Fig. S2). The relative balance between photo- and thermosensitivity is likely to be a critical trait explaining this trend. In the near future in these areas, minimum temperature are still likely to happen while dormancy induction and frost acclimation would be delayed by mean temperature increase.

Above the 14°C threshold, endodormancy induction and release would be more delayed than ecodormancy hastened, resulting in delayed budburst due to a lack of chilling, compared to the present situation. This situation would cover up to one quarter of France under RCP 8.5 scenario (Fig. 6). Although it would significantly reduce frost damages, even under false spring *scenarii*, lack of chilling would induce severe agronomic troubles such as erratic patterns of blooming, floribondity, and potential dischronism with anthesis. A similar pattern is also expected using fixed date (see Fig S3).

With respect to French nuts production, both IGP regions would face distinct threads. In the Périgord, chilling requirements are likely not to be met, and lower chilling varieties have to be selected, as the current ones do not exhibit variability for this trait (Charrier *et al.*, 2011). In Grenoble, earlier budburst dates are expected, leading to higher exposure to frost events, and

varieties with higher forcing requirements may help to stabilize the production (Charrier *et al.*, 2018). However, both regions seem relatively safe with respect to frost damages.

Conclusions and perspectives

This study highlighted the relevance of dynamic dates for simulating annual phenological cycle and frost acclimation. The DORMPHOT model, integrating temperature and photoperiodic control of dormancy induction, is the most efficient for all studied processes. On one hand, higher decennial damages would be observed in the near future on *ca.* 15% of French territory because of late frost acclimation. On the other hand, the tipping point for phenological processes is likely to be reached during the XXIst century with chilling requirements that are likely not to be fulfilled. The correlation between MAT, phenological stages and frost damages is an important tool, to build relevant meta-models at the global scale.

REFERENCES

Arora, R., Rowland, L. J., & Tanino, K. (2003). Induction and release of bud dormancy in woody perennials: a science comes of age. *HortScience*, *38*(5), 911-921.

Balandier, P., Gendraud, M., Rageau, R., Bonhomme, M., Richard, J. P., & Parisot, E. (1993). Bud break delay on single node cuttings and bud capacity for nucleotide accumulation as parameters for endo-and paradormancy in peach trees in a tropical climate. *Scientia Horticulturae*, *55*(3-4), 249-261.

Basler, D., & Körner, C. (2012). Photoperiod sensitivity of bud burst in 14 temperate forest tree species. *Agricultural and Forest Meteorology*, *165*, 73-81.

Caffarra, A., Donnelly, A., Chuine, I., & Jones, M. B. (2011a). Modelling the timing of Betula pubescens budburst. I. Temperature and photoperiod: a conceptual model. *Climate Research*, *46*(2), 147-157.

Caffarra, A., Donnelly, A., & Chuine, I. (2011b). Modelling the timing of Betula pubescens budburst. II. Integrating complex effects of photoperiod into process-based models. *Climate research*, *46*(2), 159-170.

Charrier, G., & Améglio, T. (2011). The timing of leaf fall affects cold acclimation by interactions with air temperature through water and carbohydrate contents. *Environmental and Experimental Botany*, *72*(3), 351-357.

Charrier, G., Bonhomme, M., Lacointe, A., & Améglio, T. (2011). Are budburst dates, dormancy and cold acclimation in walnut trees (Juglans regia L.) under mainly genotypic or environmental control?. *International journal of biometeorology*, *55*(6), 763-774.

Charrier, G., Chuine, I., Bonhomme, M., & Améglio, T. (2018). Assessing frost damages using dynamic models in walnut trees: exposure rather than vulnerability controls frost risks. *Plant, Cell & Environment*, *41*(5), 1008-1021.

Chuine, I., & Régnière, J. (2017). Process-based models of phenology for plants and animals. *Annual Review of Ecology, Evolution, and Systematics*, *48*, 159-182.

Chuine, I., Bonhomme, M., Legave, J. M., García de Cortázar-Atauri, I., Charrier, G., Lacointe, A., & Améglio, T. (2016). Can phenological models predict tree phenology accurately in the future? The unrevealed hurdle of endodormancy break. *Global Change Biology*, *22*(10), 3444-3460.

Delpierre, N., Dufrêne, E., Soudani, K., Ulrich, E., Cecchini, S., Boé, J., & François, C. (2009). Modelling interannual and spatial variability of leaf senescence for three deciduous tree species in France. *Agricultural and Forest Meteorology*, *149*(6-7), 938-948.

Dennis, F. G. (2003). Problems in standardizing methods for evaluating the chilling requirements for the breaking of dormancy in buds of woody plants. *HortScience*, *38*(3), 347-350.

Déqué, M., Rowell, D. P., Lüthi, D., Giorgi, F., Christensen, J. H., Rockel, B., ... & van den Hurk, B. J. J. M. (2007). An intercomparison of regional climate simulations for Europe: assessing uncertainties in model projections. *Climatic Change*, *81*(1), 53-70.

Fennell, A., & Hoover, E. (1991). Photoperiod influences growth, bud dormancy, and cold acclimation in Vitis labruscana and V. riparia. *Journal of the American Society for Horticultural Science*, *116*(2), 270-273.

Ferguson, J. C., Tarara, J. M., Mills, L. J., Grove, G. G., & Keller, M. (2011). Dynamic thermal time model of cold hardiness for dormant grapevine buds. *Annals of botany*, *107*(3), 389-396.

Gauzere, J., Lucas, C., Ronce, O., Davi, H., & Chuine, I. (2019). Sensitivity analysis of tree phenology models reveals increasing sensitivity of their predictions to winter chilling temperature and photoperiod with warming climate. *Ecological Modelling*, *411*, 108805.

Hänninen, H., & Tanino, K. (2011). Tree seasonality in a warming climate. *Trends in plant science*, *16*(8), 412-416.
Hänninen, H. (2016). Boreal and temperate trees in a changing climate. *Dordrecht: Springer. doi*, *10*, 978-94.
Heide, O. M., & Prestrud, A. K. (2005). Low temperature, but not photoperiod, controls growth cessation and dormancy induction and release in apple and pear. *Tree physiology*, *25*(1), 109-114.
Heide, O. M. (2008). Interaction of photoperiod and temperature in the control of growth and dormancy of Prunus species. *Scientia Horticulturae*, *115*(3), 309-314.
Heide, O. M. (2011). Temperature rather than photoperiod controls growth cessation and dormancy in Sorbus species. *Journal of experimental botany*, *62*(15), 5397-5404.
Kalcsits, L. A., Silim, S., & Tanino, K. (2009). Warm temperature accelerates short photoperiod-induced growth cessation and dormancy induction in hybrid poplar (Populus× spp.). *Trees*, *23*(5), 971-979.
Landsberg, J. J. (1974). Apple fruit bud development and growth; analysis and an empirical model. *Annals of Botany*, *38*(5), 1013-1023.
Lang, G. A., Early, J. D., Martin, G. C., & Darnell, R. L. (1987). Endo-, para-, and ecodormancy: physiological terminology and classification for dormancy research. *HortScience*, *22*(3), 371-377.
Leinonen, I. (1996). A simulation model for the annual frost hardiness and freeze damage of Scots pine. *Annals of Botany*, *78*(6), 687-693.
Luedeling, E. (2019) Statistical Methods for Phenology Analysis in Temperate Fruit Trees, chillR Package.
Mauget, J. C., (1980). Dormance et précocité de débourrement des bourgeons chez quelques cultivars de Noyer (Juglans regia L.).
Maurya, J. P., & Bhalerao, R. P. (2017). Photoperiod-and temperature-mediated control of growth cessation and dormancy in trees: a molecular perspective. *Annals of botany*, *120*(3), 351-360.
Mølmann, J. A., Asante, D. K., Jensen, J. B., Krane, M. N., Ernstsen, A., Junttila, O., & Olsen, J. E. (2005). Low night temperature and inhibition of gibberellin biosynthesis override phytochrome action and induce bud set and cold acclimation, but not dormancy in PHYA overexpressors and wild-type of hybrid aspen. *Plant, Cell & Environment*, *28*(12), 1579-1588.
Rageau, R. (1982). Etude expérimentale des lois d'action de la température sur la croissance des bourgeons floraux du pêcher (*Prunus* persica L. Batsch) pendant la postdormance.
Réaumur, R. A. F. d. 1735. Observations du thermomètre, faites à Paris durant l'année 1735, comparées avec celles qui ont été faites sous la ligne, à l'isle de France, à Alger et quelques unes de nos isles de l'Amérique. Mémoires de l'Académie des Sciences de Paris.
Repo, T., & Lappi, J. (1989). Estimation of standard error of impedance-estimated frost resistance. *Scandinavian Journal of Forest Research*, *4*(1-4), 67-74.
Richardson, E. A., EA, R., SD, S., & DR, W. (1974). A model for estimating the completion of rest for" Redhaven" and" Elberta" peach trees.
Vegis, A. (1964). Dormancy in higher plants. *Annual review of plant physiology*, *15*(1), 185-224.
Weinberger, J. H. (1950). Chilling requirements of peach varieties. In *Proceedings. American Society for Horticultural Science* (Vol. 56, pp. 122-8).
Weinberger, J. H. (1956). Prolonged dormancy trouble in peaches in the southeast in relation to winter temperatures. Journal of the American Society for Horticultural Science,6 7, 107-112.

Weinberger, J. H. (1967). Some temperature relations in natural breaking of the rest of Peach flower buds in the San Joaquin Valley, California. Proceedings of the American Society for Horticultural Science, 51, 84-89.

Welling, A., & Palva, E. T. (2006). Molecular control of cold acclimation in trees. *Physiologia Plantarum*, *127*(2), 167-181.

Welling, A., Kaikuranta, P., & Rinne, P. (1997). Photoperiodic induction of dormancy and freezing tolerance in Betula pubescens. Involvement of ABA and dehydrins. *Physiologia Plantarum*, *100*(1), 119-125.

Welling, A., Moritz, T., Palva, E. T., & Junttila, O. (2002). Independent activation of cold acclimation by low temperature and short photoperiod in hybrid aspen. *Plant Physiology*, *129*(4), 1633-1641.

Zhang, M. I. N., & Willison, J. H. M. (1987). An improved conductivity method for the measurement of frost hardiness. Canadian Journal of Botany, 65, 710–715.

Acknowledgements

The author wants to acknowledge the essential contribution of Marc Bonhomme, Aline Faure, Jean-Claude Mauget, Remi Rageau, Jean-Pierre Richard for dormancy release date measurements. Phenological data and stem materials were provided by Neus Aleita, Romain Baffoin, Fabrice Lheureux, Marianne Naudin and Eloise Tranchand. The author is also thankful to Thierry Améglio, André Lacointe and Heikki Hanninen for constructive comments on preliminary versions of the manuscript. Part of the collected data were supported by the Pôle National de Données de la Biodiversité (a.k.a SOERE Tempo).

Figure captions

Figure 1. A Distribution of date at the onset of chilling accumulation T_0 across France over the 1950-2005 period according to different computations: T_{min} minimum temperature (lower than 15.28°C), DP DORMPHOT model from different sets of parameters (O: original, E early, L Late), LFT_{mod} Leaf Fall model (thermal version modified), LFPT Leaf Fall model Photothermal version Original and modified. B, C and D T0 depending on mean annual temperature.

Figure 2 MTB depending on Day after September 1st (A), DS according to DP_{ori} (B), DS according to DP_L (C).

Figure 3. A-B. Average dates of endodormancy release (A) and budburst (B) predicted across France under current climatic conditions. **C-D.** Average dates of endodormancy release (C) and budburst (D) depending on mean annual temperature (°C) across France.

Figure 4. A-C. Average frost damages predicted across France under current climatic conditions in autumn (A), winter (B) and spring (C). **D.** Average early frost damages depending on the average date of the first frost lower than 0°C. **E.** Average maximum frost damages depending on the average annual minimum temperature. **F.** Average late frost damages depending on the average date of the last frost lower than -4°C.

Figure 5. A-C. Average date of onset of dormancy (A), endodormancy release (B), budburst (C) over France depending on the mean annual temperature under current climate (gray), RCP 2.6 (2006-2051 cyan, 2051-2100 blue), RCP 4.5 (2006-2051 green, 2051-2100 yellow), and RCP 8.5 *scenarii* (2006-2051 purple, 2051-2100 red). **D.** Average predicted autumn early frost damages depending on the date of first frost (<0°C) **E.** Average predicted maximum winter frost damages depending on the mean absolute minimum temperature **F.** Average predicted spring late frost damages depending on the date of last frost (<-4°C). Each dot represent the average of the considered period at 8 x 8km spatial resolution, black line represent the best non-linear regression.

Figure 6. Relative change in predicted average budburst date across France according to different climatic *scenarii* and time periods (earlier and later budburst dates than the mean are represented in blue and red, respectively).

518 **Table 1.** Site and dataset description

Location	Elevation (m asl.)	Latitude °	Longitude °	Mean annual temperature (°C)	Minimum temperature (°C)	Absolute minimum temperature (°C)	Number of freezing events	First Frost (Autumn) DOY	Last Frost (Spring) DOY	Number of observations (years and number of dates in brackets)					
										Endodormancy Release		Budburst		Frost Hardiness	
										Calibration	Validation	Calibration	Validation	Calibration	Validation
Balandran	69	43.758	4.516	16.90	12.00	-3.78	14.5	340	50	1	1	0	0	0	0
Chatte	304	45.143	5.282	13.62	8.15	-9.39	61.7	308	102	0	0	12	11	0	1 (6)
Creysse	115	44.887	1.597	14.65	8.52	-8.50	52.4	309	104	0	0	13	12	0	1 (8)
Crouël	340	45.779	3.142	13.25	9.26	-11.51	59.6	302	108	13	12	4	4	5 (49)	2 (21)
Orcival	1150	45.683	2.842	12.92	7.72	-12.13	97.4	291	126	1	1	1	0	0	0
Terrasson	90	45.136	1.300	14.61	8.96	-9.69	47.4	311	100	1	1	1	0	0	0
Theix	945	45.706	3.021	9.70	6.22	-15.11	100.3	282	129	1	1	1	0	1 (11)	1 (9)
Toulenne	22	44.557	-0.263	15.38	10.56	-6.09	25.9	325	74	1	0	9	9	0	0
Mas Bové	112	41.170	1.169	15.87	10.81	-4.05	14.9	343	47	0	0	0	0	0	1 (7)

519

520

Table 2. Quality assessment of different models. RMSE(P) less than 15% higher than minimum RMSE or RMSEP are indicated in bold.

			Endodormancy Release Date		Budburst Date		Frost Hardiness		PI
Type	Function	D_{CA}	RMSE (days)	RMSEP (days)	RMSE (days)	RMSEP (days)	RMSE (°C)	RMSEP (°C)	
Fixed		182 (Jul. 1st)	**12.84**	11.84	8.58	8.08	**1.79**	3.52	7.31
		192 (Jul. 11th)	**12.64**	11.48	8.44	**7.57**	**1.79**	3.39	7.10
		202 (Jul.21st)	**12.41**	10.73	8.25	**7.28**	**1.80**	3.42	6.94
		213 (Aug. 1st)	**12.33**	10.06	8.06	**7.14**	**1.79**	3.46	6.81
		223 (Aug. 11th)	**12.65**	**9.36**	**7.78**	**6.89**	**1.78**	3.49	6.68
		233 (Aug. 21st)	**12.68**	**8.71**	**7.61**	**6.85**	**1.78**	3.49	6.58
		244 (Sep. 1st)	**12.87**	**8.75**	**7.39**	**7.03**	**1.79**	3.48	6.59
		254 (Sep. 11th)	**13.19**	**8.49**	**7.26**	**6.88**	**1.77**	3.47	6.53
		264 (Sep. 21st)	**13.70**	**8.80**	**7.15**	**7.24**	**1.74**	3.24	6.55
		274 (Oct. 1st)	**13.80**	**8.47**	**7.25**	**7.38**	**1.73**	3.29	6.56
		284 (Oct. 11th)	13.98	**8.29**	**7.10**	**6.93**	**1.77**	3.37	6.52
		294 (Oct. 21st)	14.39	**8.47**	**7.25**	**7.15**	**1.84**	3.30	6.64
		305 (Nov. 1st)	14.48	**9.22**	**7.45**	**7.47**	**1.84**	3.21	6.78
		315 (Nov. 11th)	14.48	9.93	**7.52**	**7.56**	2.15	3.42	7.16
		325 (Nov. 21st)	14.67	10.26	**7.46**	**7.43**	2.90	3.90	7.81
		335 (Dec. 1st)	15.10	10.33	**7.58**	7.67	3.77	3.52	8.77
Dynamic	Simple	FF	17.71	14.15	9.35	15.69	**1.90**	4.92	9.84
		T_{min}	**12.88**	11.93	8.55	8.03	**1.79**	3.37	7.25
		T_{mean}	**12.93**	11.59	8.70	8.47	**1.81**	3.38	7.31
		Photoperiod	**12.31**	10.24	**7.94**	**6.85**	**1.80**	3.46	6.78
	Complex	CU_{min}	16.32	14.08	8.22	7.78	**1.78**	3.48	7.74
		LFT_{ori}	**12.91**	10.37	**8.11**	**7.23**	**1.76**	3.22	6.81
		LFT_{mod}	**12.57**	9.16	**8.11**	**7.23**	**1.80**	3.19	6.83
		$LFPT_{ori}$	**13.34**	**8.67**	**7.42**	**6.72**	**1.83**	3.24	6.51
		$LFPT_{mod}$	**12.66**	**8.81**	**7.43**	**6.89**	**1.78**	3.50	6.57
		DP_{ori}	**13.01**	**8.81**	**7.47**	**6.61**	**1.76**	**2.87**	**6.31**
		DP_E	**12.05**	**8.64**	**7.73**	**7.24**	**1.80**	3.95	6.77
		DP_L	**12.51**	**9.43**	**7.52**	**7.14**	**1.70**	**2.65**	**6.31**

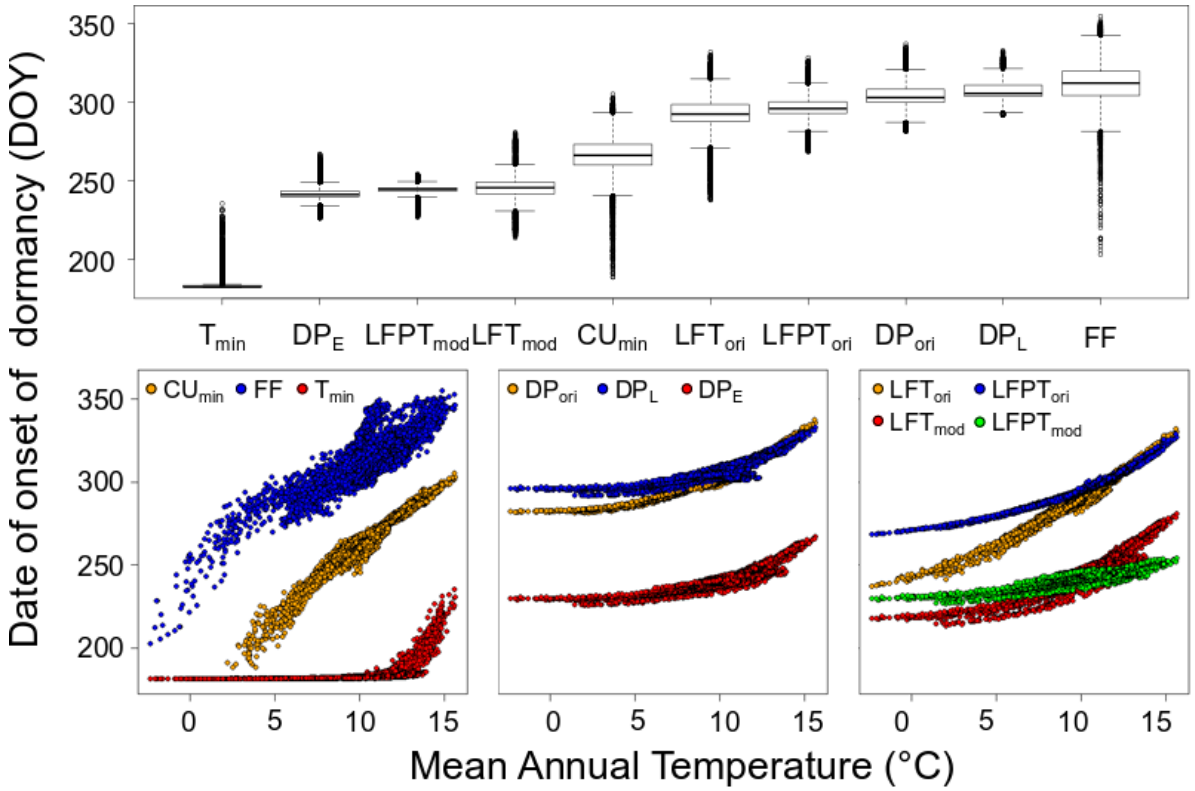

Figure 1. A Distribution of date at the onset of chilling accumulation (D_{CA}) across France over the 1950-2005 period according to different computations: T_{min} minimum temperature (lower than 15.28°C), DP DORMPHOT model from different sets of parameters (O: original, E early, L Late), LFT_{mod} Leaf Fall model (thermal version modified), LFPT Leaf Fall model Photothermal version Original and modified. B, C and D T0 depending on mean annual temperature.

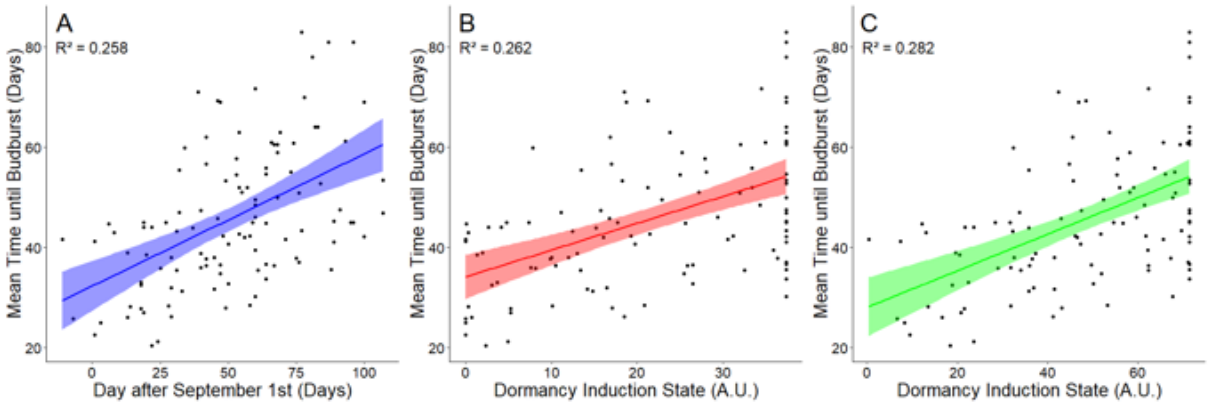

533

534 **Figure 2.** Mean time until budburst in forcing test depending on Day after September
535 1st (A), DS according to DP_{ori} (B), DS according to DP_L (C).

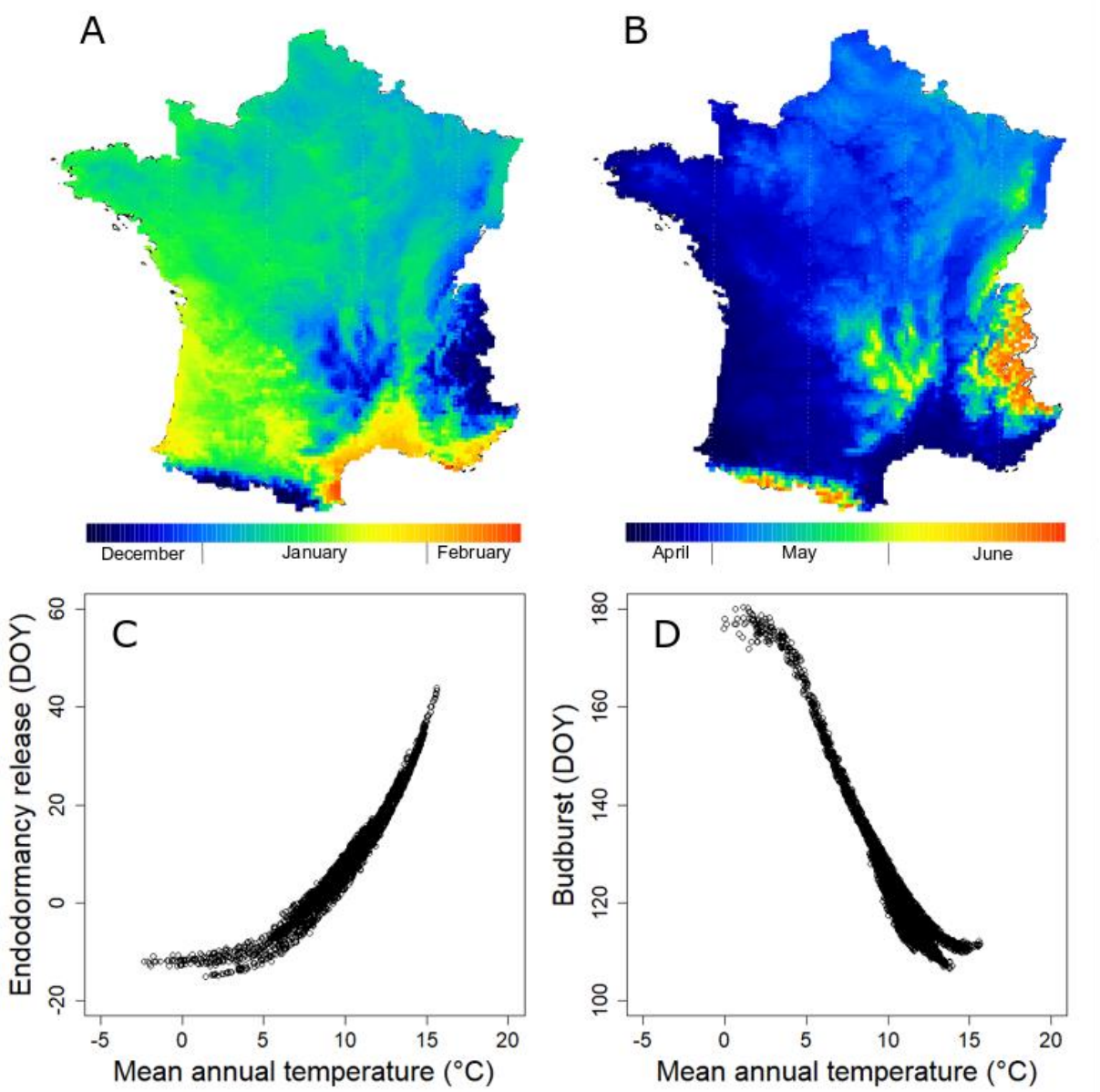

536

537 **Figure 3. A-B.** Average dates of endodormancy release (A) and budburst (B) predicted
538 across France under current climatic conditions. **C-D.** Average dates of endodormancy
539 release (C) and budburst (D) depending on mean annual temperature (°C) across
540 France.

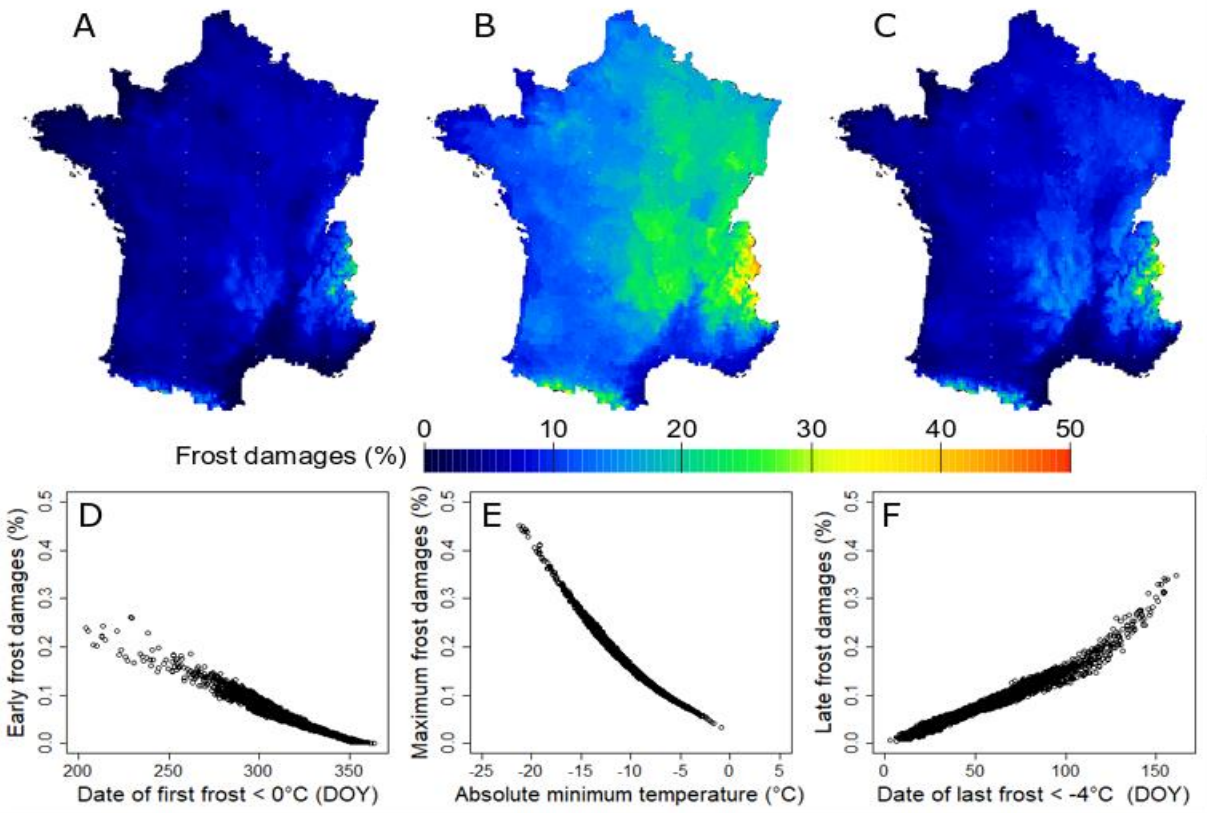

Figure 4. A-C. Average frost damages predicted across France under current climatic conditions in autumn (A), winter (B) and spring (C). **D.** Average early frost damages depending on the average date of the first frost lower than 0°C. **E.** Average maximum frost damages depending on the average annnual minimum temperature. **F.** Average late frost damages depending on the average date of the last frost lower than -4°C.

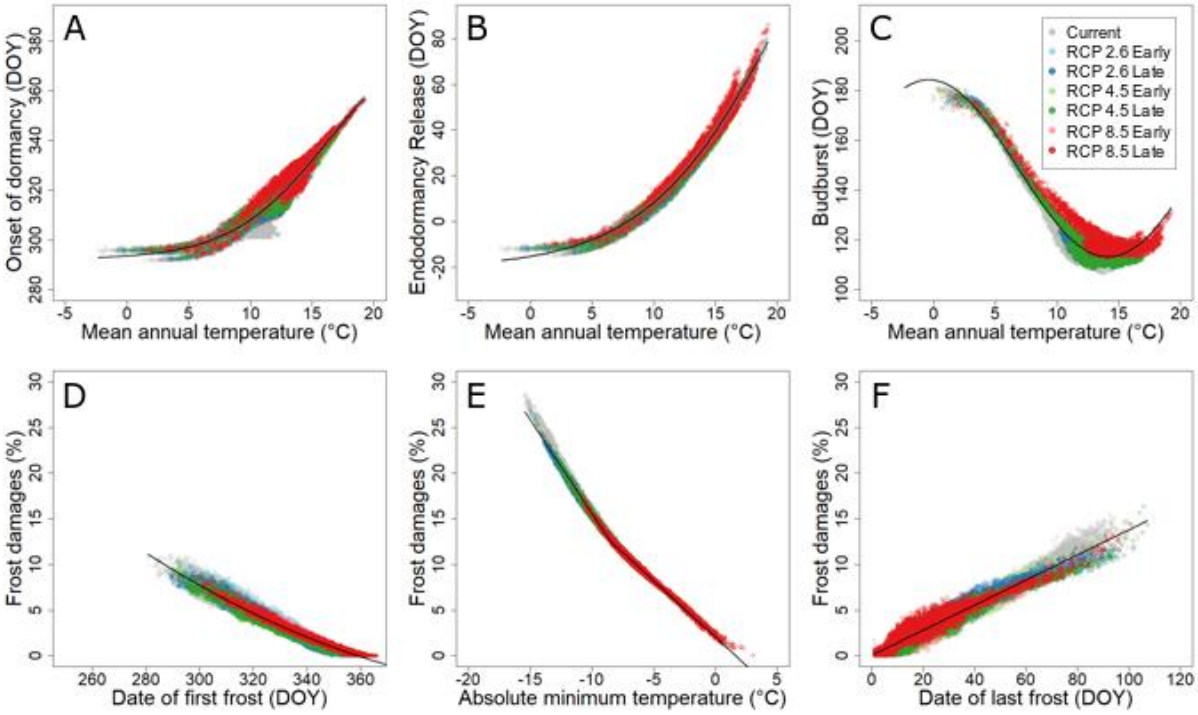

548

549 **Figure 5. A-C.** Average date of onset of dormancy (A), endodormancy release (B),
550 budburst (C) over France depending on the mean annual temperature under current
551 climate (gray), RCP 2.6 (2006-2051 cyan, 2051-2100 blue), RCP 4.5 (2006-2051
552 green, 2051-2100 yellow), and RCP 8.5 *scenarii* (2006-2051 purple, 2051-2100 red).
553 **D.** Average predicted autumn early frost damages depending on the date of first frost
554 (<0°C) **E.** Average predicted maximum winter frost damages depending on the mean
555 absolute minimum temperature **F.** Average predicted spring late frost damages
556 depending on the date of last frost (<-4°C). Each dot represent the average of the
557 considered period at 8 x 8km spatial resolution, black line represent the best non-linear
558 regression.

559

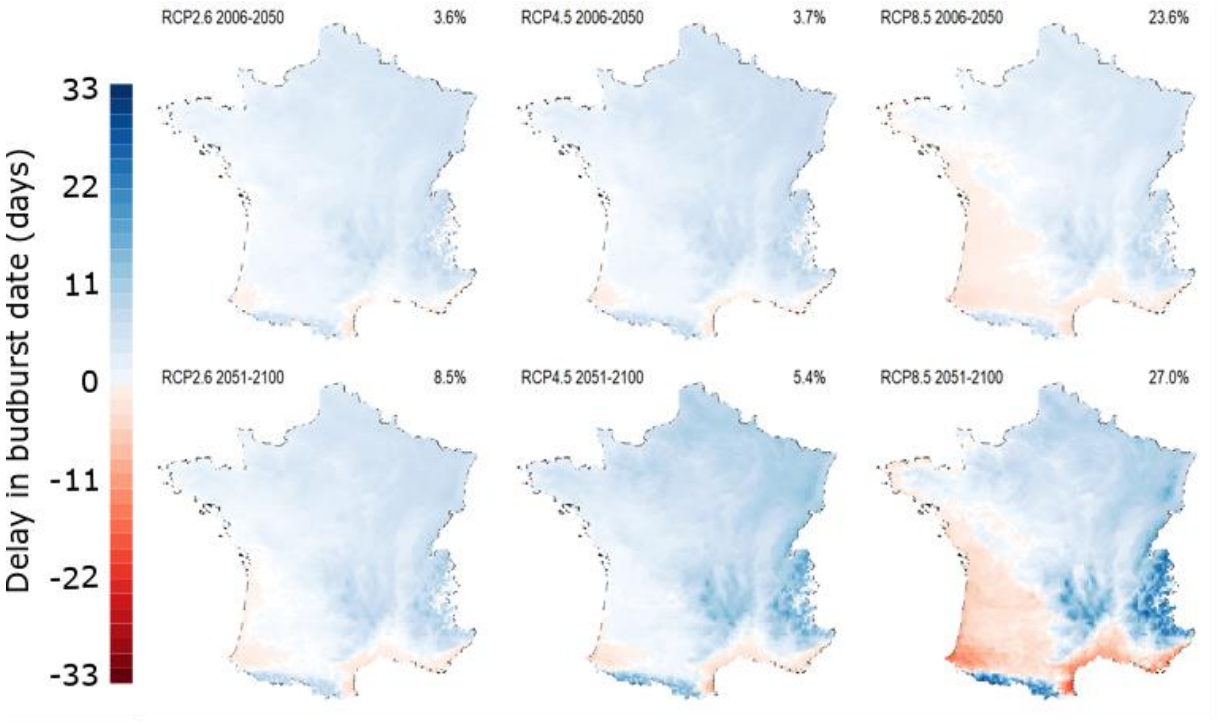

560

561 **Figure 6** Relative change in predicted average budburst date across France according
562 to different climatic *scenarii* and time periods. Earlier and later budburst dates than the
563 mean are represented in blue and red, respectively). The proportion of area showing
564 delayed budburst is indicated for each map.

565